

A FAMILY OF STABILIZER-FREE VIRTUAL ELEMENTS ON TRIANGULAR MESHES

XUEJUN XU AND SHANGYOU ZHANG

ABSTRACT. A family of stabilizer-free P_k virtual elements are constructed on triangular meshes. When choosing an accurate and proper interpolation, the stabilizer of the virtual elements can be dropped while the quasi-optimality is kept. The interpolating space here is the space of continuous P_k polynomials on the Hsieh-Clough-Tocher macro-triangle, where the macro-triangle is defined by connecting three vertices of a triangle with its barycenter. We show that such an interpolation preserves P_k polynomials locally and enforces the coercivity of the resulting bilinear form. Consequently the stabilizer-free virtual element solutions converge at the optimal order. Numerical tests are provided to confirm the theory and to be compared with existing virtual elements.

Key words. virtual element, stabilizer free, elliptic equation, Hsieh-Clough-Tocher macro-triangle, triangular mesh.

AMS subject classifications. 65N15, 65N30

1. INTRODUCTION

In this work, we construct a family of stabilizer-free P_k virtual elements ([4, 5, 9, 10, 12, 13, 14, 16, 17, 21, 22, 23]) on triangular meshes.

For solving the following model equation,

$$(1.1) \quad \begin{aligned} -\Delta u &= f \quad \text{in } \Omega, \\ u &= 0 \quad \text{on } \partial\Omega, \end{aligned}$$

where $\Omega \subset \mathbb{R}^2$ is a bounded polygonal domain and $f \in L^2(\Omega)$, the weak form reads: Find $u \in H_0^1(\Omega)$ such that

$$(1.2) \quad (\nabla u, \nabla v) = (f, v) \quad \forall v \in H_0^1(\Omega),$$

where (\cdot, \cdot) denotes the L^2 inner product on Ω and we have $|v|_1^2 = (\nabla v, \nabla v)$.

Let $\mathcal{T}_h = \{K\}$ be a quasi-uniform triangular mesh on Ω with h as the maximum size of triangles K . Let \mathcal{E}_h be the set of edges e in \mathcal{T}_h . For $k \geq 1$, the virtual element space is defined as

$$(1.3) \quad \tilde{V}_h = \{v \in H_0^1(\Omega) : \tilde{v}|_{\partial K} \in \mathbb{B}_k(\partial K), \Delta \tilde{v}|_K \in P_{k-2}(K)\},$$

where $P_{-1} = \{0\}$ and $\mathbb{B}_k(\partial K) = \{v \in C^0(\partial K) : v|_e \in P_k(e) \ \forall e \subset K\}$. In computation, the standard interpolated virtual finite element space on \mathcal{T}_h is defined by

$$(1.4) \quad V_h = \{v_h = \Pi_h^\nabla \tilde{v} : v_h|_K \in \mathbb{V}_k(K), K \in \mathcal{T}_h; \tilde{v} \in \tilde{V}_h\},$$

where $\mathbb{V}_k(K) = P_k(K)$ for the standard virtual elements (and to be defined below in (1.7) for the new method), and $v_h = \Pi_h^\nabla \tilde{v}$ satisfies, for all $w_h \in \mathbb{V}_k(K)$,

$$(1.5) \quad (v_h - \tilde{v}, w_h)_{\partial K} = 0, \quad \text{and} \quad (\nabla(v_h - \tilde{v}), \nabla w_h)_K = 0.$$

The stabilizer-free virtual element equation reads: Find $u_h = \Pi_h^\nabla \tilde{u} \in V_h$ such that

$$(1.6) \quad (\nabla u_h, \nabla v_h)_h = (f, v_h) \quad \forall \tilde{v} \in \tilde{V}_h, v_h = \Pi_h^\nabla \tilde{v},$$

where $(\nabla u_h, \nabla v_h)_h = \sum_{K \in \mathcal{T}_h} (\nabla u_h, \nabla v_h)_K$. But the dimension of V_h is less than that of \tilde{V}_h unless $k = 1$ and on triangular meshes. Thus the bilinear form in (1.6) is not coercive and the equation does not have a unique solution. A discrete stabilizer must be added to the equation (1.6).

In order to delete the stabilizer, [6] proposed to replace $\mathbb{V}_k(K) = P_k(K)$ by $\mathbb{V}_k(K) = P_{k+l}(K)$ in the virtual element space (1.4) for the case $k = 1$ on polygonal meshes, where l depends on the maximum number of edges. Further numerical tests and comparisons are given in [7]. Another stabilization-free method for $k = 1$ is proposed in [8] that $\mathbb{V}_k(K) = P_k(K) \cup H_l(K)$, where $H_l(K)$ is the set of 2D harmonic polynomials of degree l or less, and l depends on the maximum number of edges. This is an excellent idea because the H_l polynomials may enforce coerciveness while not destroying the gradient approximation, as they have vanishing Laplacian. The same idea has been implemented in some other harmonic finite elements [1, 31, 32]. But the method [8] is shown not working for $k > 3$ numerically in this paper. Another stabilizer-free virtual element method is proposed in [11] where, instead of H^1 interpolating the virtual element functions, the weak gradient (the name is used in weak Galerkin methods, and the macro-RT and macro-BDM are used to define the weak gradient in [38, 41, 45]) is defined via integration by parts and macro-mixed finite elements on polygons and polyhedra.

We propose to define the interpolation space $\mathbb{V}_k(K)$ in (1.4) as

$$(1.7) \quad \mathbb{V}_k(K) = \{v_h \in C(K) : v_h|_{K_i} \in P_k(K_i), K = \cup_{i=1}^3 K_i\},$$

where K is split in to three triangles by connecting its barycenter with three vertices, cf. Figure 1. We call K a Hsieh-Clough-Tocher macro-triangle [15, 32, 37, 48, 49].

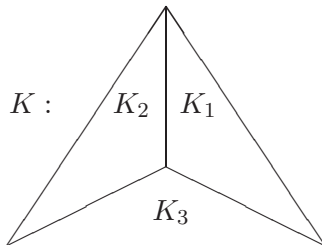


FIGURE 1. A Hsieh-Clough-Tocher macro-triangle $K = \cup_{i=1}^3 K_i$

The interpolation operator Π_h^∇ in (1.5) is naturally defined by $v_h = \Pi_h^\nabla \tilde{v} \in \mathbb{V}_k(K)$ of (1.7) satisfying

$$(1.8) \quad \begin{aligned} v_h &= \tilde{v} && \text{on } \partial K, \\ (\nabla v_h, \nabla w_h)_K &= (\nabla \tilde{v}, \nabla w_h)_K && \forall w_h \in H_0^1(K) \cap \mathbb{V}_k(K). \end{aligned}$$

We note that a different interpolation space only changes the numerical quadrature formula for computing $(\nabla u_h, \nabla v_h) = (\nabla \Pi_h^\nabla \tilde{u}, \nabla \Pi_h^\nabla \tilde{v})$ in the virtual elements equation. An accurate calculation of local interpolation does not increase the computational cost once the stiffness matrix is generated. One may see no advantage of this stabilizer-free virtual element over the Lagrange finite element. But the virtual elements are mainly for polygonal and polyhedral meshes. In [24], this stabilization technique is applied to 2D polygons and 3D polyhedra. We separate the case of triangles because it shows the idea clearly while the polygons and polyhedra have natural triangular and tetrahedral subdivisions, cf. [24].

Eliminating the stabilizer would not only reduce computational cost, but also likely to improve the condition number of the resulting system. In the numerical test, we show how the condition number of the standard virtual element is improved by three methods. But the improved condition number is still worse than that of this stabilizer-free virtual element.

Eliminating the stabilizer would likely utilize fully every degree of freedom in the discrete approximation. Thus it often leads to discoveries of superconvergence. In [25], it is shown that only this stabilizer-free P_1 virtual element converges three orders above the optimal order in H^1 -norm, and two orders above the optimal order in L^2 -norm and L^∞ -norm, when solving the Poisson equation on honeycomb meshes.

The stabilizer is eliminated first in the weak Galerkin finite element method [2, 19, 20, 26, 33, 34, 38, 39, 41], then in the $H(\text{div})$ finite element method [27, 40], in the C^0 or C^{-1} finite element methods for the biharmonic equation [43] and in the discontinuous Galerkin finite element method [18, 29]. It leads to two-order superconvergent WG finite elements [3, 35, 36, 47] and two-order superconvergent DG finite elements [44, 45] for second order elliptic equations, one or two-order superconvergent WG finite elements for the Stokes equations [28, 42], four-order superconvergent WG finite elements [46] and four-order superconvergent DG finite elements [44, 47] for the biharmonic equation. That is, for an example, a P_3 discontinuous finite element method, with the stabilizer-free technique, produces the same order approximate solution as a C^1 - P_7 finite element method does, in solving a 2D biharmonic equation.

In this paper, we show that with the new interpolation (1.8), the stabilizer-free virtual element equation (1.6) has a unique and quasi-optimal solution, on triangular meshes. Numerical tests on the new stabilizer-free virtual elements are performed. Numerical comparisons are presented, with the other stabilizer-free virtual elements and with the standard virtual elements.

2. THE WELL-POSEDNESS

We show in this section that the stabilizer-free virtual element equation has a unique solution.

Lemma 2.1. *The interpolation operator Π_h^∇ is well defined in (1.8) and it preserves P_k polynomials,*

$$(2.1) \quad \Pi_h^\nabla \tilde{v} = \tilde{v} \quad \text{if } \tilde{v} \in P_k(K).$$

Proof. Because $\tilde{v}|_{\partial K} \in \mathbb{B}_k(\partial K)$, v_h can assume the boundary condition $v_h = \tilde{v}$ exactly on ∂K . The linear system of equations in (1.8) is a finite dimensional square system. The existence is implied by the uniqueness. To show the uniqueness, we let $\tilde{v} = 0$ in (1.8). Letting $w_h = v_h$ in (1.8), we get

$$\nabla v_h = \mathbf{0} \quad \text{on } K.$$

Thus $v_h = c$ is a constant on K . As v_h is continuous on edges, $v_h = c$ is a global constant on the whole domain. By the boundary condition, we get $0 = \tilde{v}|_{\partial\Omega} = v_h|_{\partial\Omega} = c$. Hence $v_h = 0$ and (1.8) has a unique solution.

If $\tilde{v} \in P_k(K) \subset \mathbb{V}_k(K)$, defined in (1.4), then the solution of (1.8) says, letting $w_h = v_h - \tilde{v}$,

$$\nabla(v_h - \tilde{v}) = \mathbf{0}.$$

Thus $v_h - \tilde{v}$ is a global constant which must be zero as it vanishes at all ∂K . (2.1) is proved. \square

Lemma 2.2. *The stabilizer-free virtual element equation (1.6) has a unique solution, where the interpolation Π_h^∇ is defined in (1.8).*

Proof. As both $\tilde{u}, \tilde{v} \in \tilde{V}_h$, (1.6) is a finite square system of linear equations. The uniqueness of solution implies the existence. To show the uniqueness, we let $f = 0$ and $\tilde{v} = \tilde{u}$ in (1.6). It follows that

$$|\Pi_h^\nabla \tilde{u}|_{1,h} = 0.$$

Thus $\Pi_h^\nabla \tilde{u} = c$ is constant on each K . But $\Pi_h^\nabla \tilde{u}$ is continuous on the whole domain. By the boundary condition, we get $0 = \Pi_h^\nabla \tilde{u}|_{\partial\Omega} = c$. That is,

$$(2.2) \quad \Pi_h^\nabla \tilde{u} = 0.$$

On one triangle $K = \cup_{i=1}^3 K_i$,

$$(2.3) \quad \tilde{u} = \Pi_h^\nabla \tilde{u} = 0 \quad \text{on } \partial K.$$

Inside the triangle, by (1.8), (2.2), (2.3) and integration by parts, we have

$$(2.4) \quad (-\Delta \tilde{u}, w_h) = (\nabla \tilde{u}, \nabla w_h) = 0 \quad \forall w_h \in H_0^1(K) \cap \mathbb{V}_k(K).$$

By the space \tilde{V}_h definition (1.3), we denote

$$(2.5) \quad p_{k-2} = -\Delta \tilde{u} \in P_{k-2}(K).$$

Let the w_h in (2.4) be

$$(2.6) \quad w_h = p_{k-2} \phi_{\mathbf{x}_0}(\mathbf{x}) \in H_0^1(K) \cap \mathbb{V}_k(K),$$

where $\phi_{\mathbf{x}_0}(\mathbf{x})$ is the P_1 Lagrange basis function at node \mathbf{x}_0 , cf. Figure 2. That is, $\phi_{\mathbf{x}_0}(\mathbf{x})|_{K_i} = \lambda_{i,0}$ is the barycentric coordinate at x_0 on triangle K_i , i.e., a linear function which assumes value 1 at \mathbf{x}_0 and vanishing on the line e_i , cf. Figure 2.

With the w_k in (2.6), we get from (2.4) and (2.5) that

$$\int_K p_{k-2}^2 \phi_{\mathbf{x}_0}(\mathbf{x}) d\mathbf{x} = 0.$$

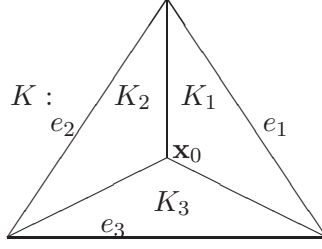


FIGURE 2. A Hsieh-Clough-Tocher macro-triangle $K = \cup_{i=1}^3 K_i$

As $\phi_{\mathbf{x}_0}(\mathbf{x}) > 0$ inside K , it follows that

$$p_{k-2}^2 = 0 \quad \text{and} \quad p_{k-2} = 0 \quad \text{on} \quad K.$$

By (2.3) and (2.5), $\Delta \tilde{u} = 0$ in K and $\tilde{u} = 0$ on ∂K . Thus, by the unique solution of the Laplace equation, $\tilde{u} = 0$. The lemma is proved. \square

3. CONVERGENCE

We prove the optimal order convergence of the stabilizer-free virtual element solutions in this section.

Theorem 3.1. *Let $u \in H^{k+1} \cap H_0^1(\Omega)$ be the exact solution of (1.2). Let u_h be the stabilizer-free virtual element solution of (1.6). It holds that*

$$(3.1) \quad |u - u_h|_1 \leq Ch^k |u|_{k+1}.$$

Proof. Since $w_h \in V_h \subset H_0^1(\Omega)$, we subtract (1.6) from (1.2) to get

$$(\nabla(u - u_h), \nabla w_h)_h = 0 \quad \forall w_h \in V_h.$$

Applying the Schwarz inequality, it follows that

$$\begin{aligned} |u - u_h|_1^2 &= (\nabla(u - u_h), \nabla(u - I_h u)) \\ &\leq |u - u_h|_1 |u - I_h u|_1 \leq Ch^k |u|_{k+1} |u - u_h|_1, \end{aligned}$$

where $I_h u$ is the Scott-Zhang interpolation on quasi-uniform triangulation \mathcal{T}_h [30]. The proof is complete. \square

To get the optimal order L^2 error bound, we need a full regularity of the dual equation that the solution of the equation,

$$\begin{aligned} -\Delta w &= g \quad \text{in} \quad \Omega, \\ w &= 0 \quad \text{on} \quad \partial\Omega, \end{aligned}$$

satisfies

$$(3.2) \quad |w|_2 \leq C\|g\|_0.$$

Theorem 3.2. *Let $u \in H^{k+1} \cap H_0^1(\Omega)$ be the exact solution of (1.2). Let u_h be the stabilizer-free virtual element solution of (1.6). Assuming (3.2), it holds that*

$$\|u - u_h\|_0 \leq Ch^{k+1}|u|_{k+1}.$$

Proof. Let $w \in H^2(\Omega) \cap H_0^1(\Omega)$ be the dual solution,

$$(3.3) \quad (\nabla w, \nabla v) = (u - u_h, v), \quad \forall v \in H_0^1(\Omega).$$

Thus, by (3.3), (3.2) and (3.1), we get

$$\begin{aligned} \|u - u_h\|_0^2 &= (\nabla w, \nabla(u - u_h)) = (\nabla(w - w_h), \nabla(u - u_h)) \\ &\leq Ch|w|_2 h^k |u|_{k+1} \leq Ch^{k+1} |u|_{k+1} \|u - u_h\|_0, \end{aligned}$$

where w_h is the virtual element solution to the equation (3.3). We obtain the L^2 error bound. \square

4. NUMERICAL TEST

We solve numerically the Poisson equation (1.1) on the domain $\Omega = (0, 1) \times (0, 1)$, where an exact solution is chosen as

$$(4.1) \quad u(x, y) = \sin(\pi x) \sin(\pi y).$$

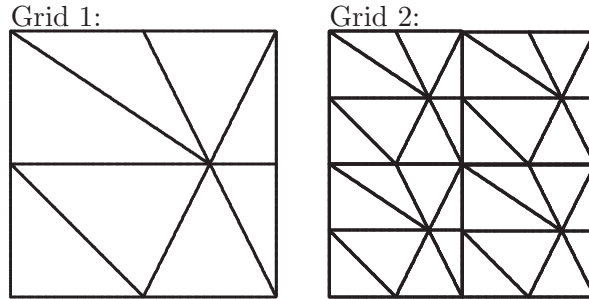


FIGURE 3. The first two levels of grids in the computation of Tables 1–4.

The computation is done first on a family of slightly irregular triangular meshes shown in Figure 3.

In Table 1, we first list the errors and the computed order of convergence for the P_1 and P_2 stabilizer-free virtual elements (1.4) with the Hsieh-Clough-Tocher macro-triangle interpolation space \mathbb{V}_k in (1.7). Optimal orders are achieved for both elements and in both L^2 and H^1 norms. Here we use $\Pi_h^\nabla u$ instead of u to check the error so that we can detect possible superconvergence. At the bottom of Table 1, we test a method of [8] where the interpolation space is $P_2 \cup H_3$, i.e., enriching the $P_2(K)$ space by two harmonic P_3 polynomials. The method is not proved yet. The numerical test shows it works well, producing optimal order errors.

TABLE 1. Error profile on Figure 3 meshes for (4.1).

Grid	$\ \Pi_h^\nabla u - u_h\ _0$	$O(h^r)$	$ \Pi_h^\nabla u - u_h _1$	$O(h^r)$
By the P_1 virtual element with HTC interpolation.				
7	0.8208E-04	2.00	0.7621E-02	1.00
8	0.2052E-04	2.00	0.3817E-02	1.00
9	0.5129E-05	2.00	0.1911E-02	1.00
By the P_2 virtual element with HTC interpolation.				
7	0.7537E-07	3.00	0.6668E-04	1.99
8	0.9423E-08	3.00	0.1670E-04	2.00
9	0.1178E-08	3.00	0.4179E-05	2.00
By the P_2 virtual element with 2 h.p. [8].				
7	0.8627E-07	3.00	0.7861E-04	2.00
8	0.1079E-07	3.00	0.1968E-04	2.00
9	0.1350E-08	3.00	0.4925E-05	2.00

In Table 2, we first list the errors and the computed order of convergence for the P_3 stabilizer-free virtual elements, $k = 3$ in (1.4) with the Hsieh-Clough-Tocher macro-triangle interpolation space \mathbb{V}_k in (1.7). Optimal orders are achieved for the element in both L^2 and H^1 norms. At the bottom of Table 2, we test a method of [8] where the interpolation space is $P_3 \cup H_5$, i.e., enriching the $P_3(K)$ polynomial space by four harmonic P_4 and P_5 polynomials. The method is not proved yet. The numerical test shows it works well, producing optimal order errors.

In Table 3, we first list the errors and the computed orders of convergence for the P_4 stabilizer-free virtual elements, $k = 4$ in (1.4) with the Hsieh-Clough-Tocher macro-triangle interpolation space \mathbb{V}_k in (1.7). Optimal orders are achieved for the element in both L^2 and H^1 norms. Here the

TABLE 2. Error profile on Figure 3 meshes for (4.1).

Grid	$\ \Pi_h^\nabla u - u_h\ _0$	$O(h^r)$	$ \Pi_h^\nabla u - u_h _1$	$O(h^r)$
	By the P_3 virtual element with HTC interpolation.			
6	0.4664E-08	4.00	0.3068E-05	2.99
7	0.2916E-09	4.00	0.3844E-06	3.00
8	0.1824E-10	4.00	0.4811E-07	3.00
	By the P_3 virtual element with 8 h.p. [8].			
6	0.5676E-08	4.01	0.3392E-05	2.99
7	0.3542E-09	4.00	0.4257E-06	2.99
8	0.2222E-10	3.99	0.5372E-07	2.99

computer accuracy is exhausted when computing the last grid solution. At the bottom of Table 3, we test a method of [8] where the interpolation space is $P_4 \cup H_{10}$, i.e., enriching the $P_4(K)$ polynomial space by 12 harmonic P_5 , $P - 6$, P_7 , P_8 , P_9 and P_{10} polynomials. Since the method does not work, we tested by adding more harmonic polynomials until the error can not be reduced anymore.

TABLE 3. Error profile on Figure 3 meshes for (4.1).

Grid	$\ \Pi_h^\nabla u - u_h\ _0$	$O(h^r)$	$ \Pi_h^\nabla u - u_h _1$	$O(h^r)$
	By the P_4 virtual element with HTC interpolation.			
5	0.7612E-09	5.00	0.3811E-06	3.99
6	0.2374E-10	5.00	0.2389E-07	4.00
7	0.7616E-12	—	0.1495E-08	4.00
	By the P_4 virtual element with 12 h.p. [8].			
4	0.4589E-07	5.01	0.7336E-05	3.94
5	0.1525E-08	4.91	0.5830E-06	3.65
6	0.9493E-10	4.01	0.9239E-07	2.66

In Table 4, we first list the errors and the computed orders of convergence for the P_5 stabilizer-free virtual elements, $k = 5$ in (1.4) with the Hsieh-Clough-Tocher macro-triangle interpolation space \mathbb{V}_k in (1.7). Optimal orders are achieved for the element in both L^2 and H^1 norms. At the middle of Table 4, we test a method of [8] where the interpolation space is $P_5 \cup H_{10}$, i.e., enriching the $P_5(K)$ polynomial space by 10 harmonic P_6 , P_7 , P_8 , P_9 and P_{10} polynomials. Since the method does not work, we tested by

adding more harmonic polynomials until the error can not be reduced anymore. Comparing to the last case, the convergent order deteriorates a lot. At the bottom of Table 4, we list the errors and the computed orders of convergence for the P_6 stabilizer-free virtual elements, $k = 6$ in (1.4) with the Hsieh-Clough-Tocher macro-triangle interpolation space \mathbb{V}_k in (1.7). Optimal orders are achieved for the element in both L^2 and H^1 norms.

TABLE 4. Error profile on Figure 3 meshes for (4.1).

Grid	$\ \Pi_h^\nabla u - u_h\ _0$	$O(h^r)$	$\ \Pi_h^\nabla u - u_h\ _1$	$O(h^r)$
By the P_5 virtual element with HTC interpolation.				
3	0.3339E-07	6.01	0.5275E-05	4.96
4	0.5170E-09	6.01	0.1665E-06	4.99
5	0.8033E-11	6.01	0.5223E-08	4.99
By the P_5 virtual element with 10 h.p. [8].				
2	0.4262E-05	5.18	0.2158E-03	4.24
3	0.1566E-06	4.77	0.2319E-04	3.22
4	0.1819E-07	3.11	0.5702E-05	2.02
By the P_6 virtual element with HTC interpolation.				
2	0.1696E-06	7.30	0.1576E-04	6.19
3	0.1320E-08	7.01	0.2515E-06	5.97
4	0.1025E-10	7.01	0.3956E-08	5.99

The next part of computation is done on the uniform triangular meshes, shown as in Figure 4. This is mainly for detecting possible superconvergence.

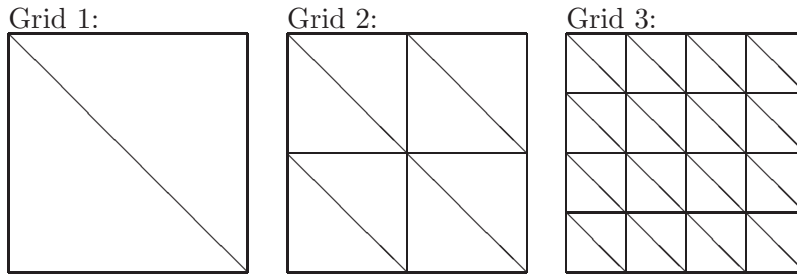


FIGURE 4. The first three levels of grids for the computation in Tables 5–7.

In Table 5, we first list the errors and the computed orders of convergence for the P_1 stabilizer-free virtual elements, $k = 1$ in (1.4) with the

Hsieh-Clough-Tocher macro-triangle interpolation space \mathbb{V}_k in (1.7). Optimal orders are achieved for the element in both L^2 and H^1 norms. In fact, we have one-order superconvergence in H^1 semi-norm. At the bottom of Table 5, we list the errors and the computed orders of convergence for the P_1 standard virtual elements, $k = 1$ in (1.4). Optimal orders are achieved for the element in both L^2 and H^1 norms. Again, we have one-order H^1 superconvergence for this element. Comparing the errors, the new method is slightly better which is understandable as their interpolation space $P_1(K)$ is a subspace of our interpolation space $\mathbb{V}_1 = C(K) \cap \cup_{i=1}^3 P_1(K_i)$.

TABLE 5. Error profile on Figure 4 meshes for (4.1).

Grid	$\ \Pi_h^\nabla u - u_h\ _0$	$O(h^r)$	$ \Pi_h^\nabla u - u_h _1$	$O(h^r)$
	By the P_1 SF virtual element with HTC interpolation.			
7	0.3032E-03	2.00	0.1382E-02	2.00
8	0.7586E-04	2.00	0.3457E-03	2.00
9	0.1897E-04	2.00	0.8644E-04	2.00
	By the standard P_1 virtual element [4].			
6	0.1210E-02	1.98	0.5518E-02	1.99
7	0.3032E-03	2.00	0.1382E-02	2.00
8	0.7586E-04	2.00	0.3457E-03	2.00

In Table 6, we first list the errors and the computed orders of convergence for the P_2 stabilizer-free virtual elements, $k = 2$ in (1.4) with the Hsieh-Clough-Tocher macro-triangle interpolation space \mathbb{V}_k in (1.7). Optimal orders are achieved for the element in both L^2 and H^1 norms. Unlike the traditional P_2 finite element, we do not have any superconvergence. Comparing to the traditional P_2 finite element, we compute a solution in a larger vector space but get a worse result. This is because the added Hsieh-Clough-Tocher macro-bubbles destroy the symmetry of P_2 finite element equations on uniform triangular meshes. At the bottom of Table 6, we list the errors and the computed orders of convergence for the standard P_2 virtual elements, $k = 2$ in (1.4). Optimal orders are achieved for the element in both L^2 and H^1 norms. Comparing the two errors, the new method is much better which is understandable as there is no stabilizer here.

In Table 7, we list the errors and the computed orders of convergence for the P_3 , P_4 , P_5 and P_6 stabilizer-free virtual elements, $k = 3, 4, 5$, or 6 in (1.4) with the Hsieh-Clough-Tocher macro-triangle interpolation space

TABLE 6. Error profile on Figure 4 meshes for (4.1).

Grid	$\ \Pi_h^\nabla u - u_h\ _0$	$O(h^r)$	$ \Pi_h^\nabla u - u_h _1$	$O(h^r)$
By the P_2 SF virtual element with HTC interpolation.				
7	0.5604E-07	3.72	0.2302E-04	2.48
8	0.5261E-08	3.41	0.4990E-05	2.21
9	0.5901E-09	3.16	0.1194E-05	2.06
By the standard P_2 virtual element [4].				
6	0.1885E-05	3.15	0.3225E-03	2.08
7	0.2285E-06	3.04	0.7958E-04	2.02
8	0.2833E-07	3.01	0.1983E-04	2.00

\mathbb{V}_k in (1.7). Optimal orders are achieved for all the elements in both L^2 and H^1 norms. Comparing the errors of same virtual elements, the uniform triangular meshes are much better than the triangular meshes shown in Figure 3.

TABLE 7. Error profile on Figure 3 meshes for (4.1).

Grid	$\ \Pi_h^\nabla u - u_h\ _0$	$O(h^r)$	$ \Pi_h^\nabla u - u_h _1$	$O(h^r)$
By the P_3 SF virtual element with HTC interpolation.				
6	0.4906E-07	3.98	0.1628E-04	2.98
7	0.3087E-08	3.99	0.2048E-05	2.99
8	0.1935E-09	4.00	0.2567E-06	3.00
By the P_4 SF virtual element with HTC interpolation.				
5	0.1038E-07	5.03	0.3216E-05	4.00
6	0.3216E-09	5.01	0.2011E-06	4.00
7	0.1001E-10	5.01	0.1258E-07	4.00
By the P_5 SF virtual element with HTC interpolation.				
5	0.2035E-09	6.00	0.7749E-07	4.98
6	0.3173E-11	6.00	0.2433E-08	4.99
7	0.5018E-13	5.98	0.7612E-10	5.00
By the P_6 SF virtual element with HTC interpolation.				
3	0.5536E-07	6.99	0.5949E-05	5.94
4	0.4294E-09	7.01	0.9376E-07	5.99
5	0.3333E-11	7.01	0.1468E-08	6.00

We would compare more the stabilizer-free virtual element with the standard virtual elements of [4]. The standard H^1 interpolation is defined by

$\Pi_h^1 \tilde{u} \in P_k(K)$ such that

$$(4.2) \quad \begin{aligned} (\nabla \Pi_h^1 \tilde{u}, \nabla p)_K &= -(\tilde{u}, \Delta p)_K + \langle \tilde{u}, \nabla p \cdot \mathbf{n} \rangle_{\partial K} \quad \forall p \in P_k(K) \setminus P_0(K), \\ \langle \Pi_h^1 \tilde{u}, p \rangle_{\partial K} &= \langle \tilde{u}, p \rangle_{\partial K} \quad \forall p \in P_0(K), \end{aligned}$$

where \mathbf{n} is the unit outer normal vector. \tilde{u} is defined by the degrees of freedom on triangle $K = \mathbf{x}_1 \mathbf{x}_2 \mathbf{x}_3$, $\{F_i, i = 1, \dots, N_K\}$, cf. [4],

$$(4.3) \quad F_i(\tilde{u}) = \begin{cases} \tilde{u}(\mathbf{x}_j), & j = 1, 2, 3, \\ \tilde{u}\left(\frac{l\mathbf{x}_j + (k-l)\mathbf{x}_{\text{mod}(j,3)+1}}{k}\right), & l = 1, \dots, k-1; j = 1, 2, 3, \\ \frac{\int_K \tilde{u}(x-x_0)^j (y-y_0)^l d\mathbf{x}}{\int_K 1 d\mathbf{x}}, & 0 \leq j+l \leq k-2, \end{cases}$$

where $\mathbf{x}_0 = (x_0, y_0)$ is the barycenter of K . The standard stabilizer in [4] is defined as

$$(4.4) \quad S(\tilde{u} - \Pi_h^1 \tilde{u}, \tilde{v} - \Pi_h^1 \tilde{v})_K = \sum_{i=1}^{N_K} F_i(\tilde{u} - \Pi_h^1 \tilde{u}) F_i(\tilde{v} - \Pi_h^1 \tilde{v}).$$

In Table 8, we compute the solution (4.1) again by the HTC-interpolating VM method and by the standard virtual element method [4] defined by (4.2), (4.3) and (4.4). We first read the condition number $\kappa_2(A)$ in l^2 norm for the stiffness matrix A in Table 8. We can see the condition number is huge for the [4] P_3 VM, with (4.3) and (4.4). It would make a direct solver fail on higher level meshes. When we read the stiffness matrix of the [4] P_3 VM, we find the term for the basis function associate with $(x - x_0)^1$ -moment is much bigger than that with $(x - x_0)^0$ -moment. Therefore we replace the degrees of freedom (4.3) by a better scaled set,

$$(4.5) \quad F_i(\tilde{u}) = \begin{cases} \tilde{u}(\mathbf{x}_j), & j = 1, 2, 3, \\ \tilde{u}\left(\frac{l\mathbf{x}_j + (k-l)\mathbf{x}_{\text{mod}(j,3)+1}}{k}\right), & l = 1, \dots, k-1; j = 1, 2, 3, \\ \frac{\int_K \tilde{u}(x-x_0)^j (y-y_0)^l d\mathbf{x}}{(\int_K [(x-x_0)^j (y-y_0)^l]^2 d\mathbf{x})^{1/2}}, & 0 \leq j+l \leq k-2. \end{cases}$$

The condition number of the [4] P_3 VM (with (4.5) and (4.4)) is improved, see the third part of Table 8. When we read the new stiffness matrix of the [4] P_3 VM, we find the term for the basis function associate with $(x - x_0)^0$ -moment is much bigger than that with the degree of freedom $\tilde{u}(\mathbf{x}_1)$. Therefore we scale the degrees of freedom (4.3) again,

$$(4.6) \quad F_i(\tilde{u}) = \begin{cases} \tilde{u}(\mathbf{x}_j), & j = 1, 2, 3, \\ \tilde{u}\left(\frac{l\mathbf{x}_j + (k-l)\mathbf{x}_{\text{mod}(j,3)+1}}{k}\right), & l = 1, \dots, k-1; j = 1, 2, 3, \\ \frac{10 \int_K \tilde{u}(x-x_0)^j (y-y_0)^l d\mathbf{x}}{(\int_K [(x-x_0)^j (y-y_0)^l]^2 d\mathbf{x})^{1/2}}, & 0 \leq j+l \leq k-2. \end{cases}$$

The condition number is reduced again, seen in the fourth part of Table 8. This is nearly the best we can do about the conditioning. It is better only at the first level than the new virtual element's condition number. Supposedly, changing the basis does not change the solution. But here the error of the solution in the fourth part of Table 8 is changed (smaller). It indicates that the bad condition number of the [4] P_3 VM does increase round-off errors.

TABLE 8. Error profile on Figure 3 meshes for (4.1).

Grid	$\ \Pi_h^\nabla u - u_h\ _0$	$O(h^r)$	$ \Pi_h^\nabla u - u_h _1$	$O(h^r)$	$\kappa_2(A)$
By the P_3 virtual element with HTC interpolation.					
1	0.3607E-02	0.00	0.6845E-01	0.00	0.6783E+03
2	0.2967E-03	3.60	0.1129E-01	2.60	0.7205E+03
3	0.1890E-04	3.97	0.1510E-02	2.90	0.7273E+03
4	0.1190E-05	3.99	0.1934E-03	2.96	0.1204E+04
5	0.7456E-07	4.00	0.2443E-04	2.98	0.4812E+04
By the [4] P_3 VM, with (4.3) and (4.4).					
1	0.4093E-02	0.00	0.7393E-01	0.00	0.7286E+05
2	0.4283E-03	3.26	0.1361E-01	2.44	0.3420E+06
3	0.3187E-04	3.75	0.2224E-02	2.61	0.1353E+07
4	0.3037E-05	3.39	0.4359E-03	2.35	0.5400E+07
By the [4] P_3 VM, with (4.5) and (4.4).					
1	0.4093E-02	0.00	0.7393E-01	0.00	0.6325E+04
2	0.4283E-03	3.26	0.1361E-01	2.44	0.2749E+05
3	0.3187E-04	3.75	0.2224E-02	2.61	0.1070E+06
4	0.3037E-05	3.39	0.4359E-03	2.35	0.4253E+06
By the [4] P_3 VM, with (4.6) and (4.4).					
1	0.4089E-02	0.00	0.7384E-01	0.00	0.3581E+03
2	0.4278E-03	3.26	0.1359E-01	2.44	0.1530E+04
3	0.3176E-04	3.75	0.2216E-02	2.62	0.6073E+04
4	0.3018E-05	3.40	0.4332E-03	2.35	0.2424E+05

The [4] P_3 virtual element solution does not converge at the correct order in Table 8. This problem does not happen to the P_1 and P_2 VM solutions, cf. Tables 5 and 6. Thus we increase the power of the stabilizer $S(\cdot, \cdot)_K$ in

(4.4) by a scaling,

$$(4.7) \quad S(\tilde{u} - \Pi_h^1 u, \tilde{v} - \Pi_h^1 v)_K = h^\alpha \sum_{i=1}^{N_K} F_i(\tilde{u} - \Pi_h^1 u) F_i(\tilde{v} - \Pi_h^1 v),$$

where α is to be specified, depending on the polynomial degree k . In Table 9, the error and the computed order of convergence are listed for the [4] P_3 VM, with stabilizer's $\alpha = 0$ and -1 in (4.7). We can see, for the latter, the method can converge at the optimal order. The errors of the stabilizer-free VM are slightly smaller, see Table 2.

TABLE 9. Error profile on Figure 3 meshes for (4.1).

Grid	$\ \Pi_h^\nabla u - u_h\ _0$	$O(h^r)$	$ \Pi_h^\nabla u - u_h _1$	$O(h^r)$
By the [4] P_3 VM, with (4.6) and (4.7), $\alpha = 0$.				
1	0.4089E-02	0.00	0.7384E-01	0.00
2	0.4278E-03	3.26	0.1359E-01	2.44
3	0.3176E-04	3.75	0.2216E-02	2.62
4	0.3018E-05	3.40	0.4332E-03	2.35
By the [4] P_3 VM, with (4.6) and (4.7), $\alpha = -1$.				
1	0.4093E-02	0.00	0.7393E-01	0.00
2	0.4069E-03	3.33	0.1261E-01	2.55
3	0.2529E-04	4.01	0.1681E-02	2.91
4	0.1583E-05	4.00	0.2172E-03	2.95
5	0.9949E-07	3.99	0.2765E-04	2.97
6	0.6245E-08	3.99	0.3491E-05	2.99

In Table 10, the error and the computed order of convergence are listed for the [4] P_4 VM, with stabilizer's $\alpha = 0, -1$ and -2 in (4.7). We can see that the standard stabilizer (4.4) does not work when $k = 4$. We can see, for the last $\alpha = -2$ (depending on polynomial degree $k = 4$ here), the method does converge at the optimal order, in Table 10. The errors of the stabilizer-free VM are slightly smaller, see Table 3.

5. ETHICAL STATEMENT

5.1. Compliance with Ethical Standards.

The submitted work is original and is not published elsewhere in any form or language.

TABLE 10. Error profile on Figure 3 meshes for (4.1).

Grid	$\ \Pi_h^\nabla u - u_h\ _0$	$O(h^r)$	$ \Pi_h^\nabla u - u_h _1$	$O(h^r)$
By the [4] P_4 VM, with (4.6) and (4.7), $\alpha = 0$.				
1	0.1655E-02	0.00	0.3146E-01	0.00
2	0.8753E-04	4.24	0.3987E-02	2.98
3	0.1025E-04	3.09	0.9204E-03	2.12
4	0.1298E-05	2.98	0.2294E-03	2.00
By the [4] P_4 VM, with (4.6) and (4.7), $\alpha = -1$.				
1	0.1655E-02	0.00	0.3146E-01	0.00
2	0.6940E-04	4.58	0.3162E-02	3.31
3	0.5106E-05	3.76	0.4866E-03	2.70
4	0.3993E-06	3.68	0.7665E-04	2.67
By the [4] P_4 VM, with (4.6) and (4.7), $\alpha = -1$.				
1	0.1655E-02	0.00	0.3146E-01	0.00
2	0.5695E-04	4.86	0.2511E-02	3.65
3	0.2260E-05	4.66	0.2115E-03	3.57
4	0.7827E-07	4.85	0.1489E-04	3.83
5	0.2514E-08	4.96	0.9577E-06	3.96
6	0.7946E-10	4.98	0.6012E-07	3.99

5.2. Funding.

Xuejun Xu was supported by National Natural Science Foundation of China (Grant No. 12071350), Shanghai Municipal Science and Technology Major Project No. 2021SHZDZX0100, and Science and Technology Commission of Shanghai Municipality.

5.3. Conflict of Interest.

There is no potential conflict of interest .

5.4. Ethical approval.

This article does not contain any studies involving animals. This article does not contain any studies involving human participants.

5.5. Informed consent.

This research does not have any human participant.

5.6. Availability of supporting data.

This research does not use any external or author-collected data.

5.7. Authors' contributions.

All authors made equal contribution.

5.8. Acknowledgments.

None.

REFERENCES

- [1] A. Al-Twaeel, Y. Dong, S. Hussain and X. Wang, A weak Galerkin harmonic finite element method for Laplace equation, *Commun. Appl. Math. Comput.* 3 (2021), no. 3, 527–543.
- [2] A. Al-Twaeel, S. Hussain and X. Wang, A stabilizer free weak Galerkin finite element method for parabolic equation, *J. Comput. Appl. Math.*, 392 (2021), 113373.
- [3] A. Al-Twaeel, X. Wang, X. Ye and S. Zhang, A stabilizer free weak Galerkin element method with supercloseness of order two, *Numer. Methods Partial Differential Equations* 37 (2021), no. 2, 1012–1029.
- [4] L. Beirão da Veiga, F. Brezzi, A. Cangiani, G. Manzini, L. D. Marini and A. Russo, Basic principles of virtual element methods, *Math. Models Methods Appl. Sci.* 23 (2013) 199–214.
- [5] L. Beirão da Veiga, F. Brezzi, L. D. Marini and A. Russo, H(div) and H(curl)-conforming virtual element methods, *Numer. Math.* 133 (2016) 303–332.
- [6] S. Berrone, A. Borio, F. Marcon and G. Teora, A first-order stabilization-free virtual element method, *Appl. Math. Lett.* 142 (2023), Paper No. 108641, 6 pp.
- [7] S. Berrone, A. Borio and F. Marcon, Comparison of standard and stabilization free Virtual Elements on anisotropic elliptic problems, 2022, arXiv:2202.08571v1.
- [8] S. Berrone, A. Borio and F. Marcon, Lowest order stabilization free Virtual Element Method for the Poisson equation, 2023, arXiv:2103.16896v1.
- [9] S. Cao, L. Chen and R. Guo, A virtual finite element method for two-dimensional Maxwell interface problems with a background unfitted mesh, *Math. Models Methods Appl. Sci.* 31 (2021), no. 14, 2907–2936.
- [10] S. Cao, L. Chen and R. Guo, Immersed virtual element methods for electromagnetic interface problems in three dimensions, *Math. Models Methods Appl. Sci.* 33 (2023), no. 3, 455–503.
- [11] C. Chen, X. Huang and H. Wei, Virtual Element Methods Without Extrinsic Stabilization, 2023, arXiv:2212.01720v4.
- [12] L. Chen, H. Wei and M. Wen, An interface-fitted mesh generator and virtual element methods for elliptic interface problems, *J. Comput. Phys.* 334 (2017), 327–348.
- [13] L. Chen and J. Huang, Some error analysis on virtual element methods, *Calcolo* 55 (2018), no. 1, Paper No. 5, 23 pp.
- [14] L. Chen and X. Huang, Nonconforming virtual element method for 2mth order partial differential equations in \mathbb{R}^n , *Math. Comp.* 89 (2020), no. 324, 1711–1744.
- [15] R.W. Clough and J.L. Tocher, Finite element stiffness matrices for analysis of plates in bending, in: *Proceedings of the Conference on Matrix Methods in Structural Mechanics*, Wright Patterson A.F.B. Ohio, 1965.
- [16] F. Feng, W. Han and J. Huang, Virtual element methods for elliptic variational inequalities of the second kind, *J. Sci. Comput.* 80 (2019), no. 1, 60–80.
- [17] F. Feng, J. Huang and Y. Yu, A non-consistent virtual element method for reaction diffusion equations, *East Asian J. Appl. Math.* 10 (2020), no. 4, 786–799.
- [18] Y. Feng, Y. Liu, R. Wang and S. Zhang, A conforming discontinuous Galerkin finite element method on rectangular partitions, *Electron. Res. Arch.* 29 (2021), no. 3, 2375–2389.

- [19] Y. Feng, Y. Liu, R. Wang and S. Zhang, A stabilizer-free weak Galerkin finite element method for the Stokes equations, *Adv. Appl. Math. Mech.* 14 (2022), no. 1, 181–201.
- [20] F. Gao, X. Ye and S. Zhang, A discontinuous Galerkin finite element method without interior penalty terms, *Adv. Appl. Math. Mech.* 14 (2022), no. 2, 299–314.
- [21] J. Huang and S. Lin, A C^0P_2 time-stepping virtual element method for linear wave equations on polygonal meshes, *Electron. Res. Arch.* 28 (2020), no. 2, 911–933.
- [22] J. Huang and Y. Yu, Some estimates for virtual element methods in three dimensions, *Comput. Methods Appl. Math.* 23 (2023), no. 1, 177–187.
- [23] J. Huang and Y. Yu, A medius error analysis for nonconforming virtual element methods for Poisson and biharmonic equations, *J. Comput. Appl. Math.* 386 (2021), Paper No. 113229, 20 pp.
- [24] Y. Lin, M. Mu and S. Zhang, Stabilizer-free polygonal and polyhedral virtual elements, 2023, arXiv:2309.10250.
- [25] Y. Lin, M. Mu and S. Zhang, Superconvergent P1 honeycomb virtual elements and lifted P3 solutions, 2023, arXiv:submit/5228902.
- [26] L. Mu, X. Ye and S. Zhang, A stabilizer free, pressure robust and superconvergence weak Galerkin finite element method for the Stokes Equations on polytopal mesh, *SIAM J. Sci. Comput.*, 43 (2021), A2614–A2637.
- [27] L. Mu, X. Ye and S. Zhang, Development of pressure-robust discontinuous Galerkin finite element methods for the Stokes problem, *J. Sci. Comput.* 89 (2021), no. 1, Paper No. 26, 25 pp.
- [28] L. Mu, X. Ye and S. Zhang, A stabilizer free, pressure robust, and superconvergence weak Galerkin finite element method for the Stokes Equations on polytopal mesh, *SIAM J. Sci. Comput.* 43 (2021), no. 4, A2614–A2637.
- [29] L. Mu, X. Ye, S. Zhang and P. Zhu, A DG method for the Stokes equations on tensor product meshes with $[P_k]^d - P_{k-1}$ element, *Communications on Applied Mathematics and Computation*, 2023, doi:10.1007/s42967-022-00243-9.
- [30] L. R. Scott and S. Zhang, Finite element interpolation of nonsmooth functions satisfying boundary conditions, *Math. Comp.* 54 (1990), no. 190, 483–493.
- [31] T. Sorokina and S. Zhang, Conforming and nonconforming harmonic finite elements, *Appl. Anal.* 99 (2020), no. 4, 569–584.
- [32] T. Sorokina and S. Zhang, Conforming harmonic finite elements on the Hsieh-Clough-Tocher split of a triangle, *Int. J. Numer. Anal. Model.* 17 (2020), no. 1, 54–67.
- [33] J. Wang, X. Ye and S. Zhang, Numerical investigation on weak Galerkin finite elements, *Int. J. Numer. Anal. Model.* 17 (2020) no. 4, 517–531.
- [34] J. Wang, X. Ye and S. Zhang, Weak Galerkin finite element methods with or without stabilizers, *Numer. Algorithms* 88 (2021), no. 3, 1361–1381.
- [35] J. Wang, X. Wang, X. Ye, S. Zhang and P. Zhu, Two-order superconvergence for a weak Galerkin method on rectangular and cuboid grids, *Numer. Methods Partial Differential Equations* 39 (2023), no. 1, 744–758.
- [36] J. Wang, X. Wang, X. Ye, S. Zhang and P. Zhu, On the superconvergence of a WG method for elliptic problem with variable coefficients, *Science China*, 2023, doi:10.1007/s11425-022-2097-8.
- [37] X. Xu and S. Zhang, A new divergence-free interpolation operator with applications to the Darcy-Stokes-Brinkman equations, *SIAM J. Sci. Comput.* 32 (2010), no. 2, 855–874.
- [38] X. Ye and S. Zhang, A stabilizer-free weak Galerkin finite element method on polytopal meshes, *J. Comput. Appl. Math.* 371 (2020), 112699, 9 pp.
- [39] X. Ye and S. Zhang, A Stabilizer Free Weak Galerkin Method for the Biharmonic Equation on Polytopal Meshes, *SIAM J. Numer. Anal.* 58 (2020), no. 5, 2572–2588.
- [40] X. Ye and S. Zhang, A stabilizer-free pressure-robust finite element method for the Stokes equations, *Adv. Comput. Math.* 47 (2021), no. 2, Paper No. 28, 17 pp.

- [41] X. Ye and S. Zhang, A stabilizer free weak Galerkin finite element method on polytopal mesh: Part III, *J. Comput. Appl. Math.* 394 (2021), Paper No. 113538, 9 pp.
- [42] X. Ye and S. Zhang, A stabilizer free WG Method for the Stokes Equations with order two superconvergence on polytopal mesh, *Electron. Res. Arch.* 29 (2021), no. 6, 3609–3627.
- [43] X. Ye and S. Zhang, A C^0 -conforming DG finite element method for biharmonic equations on triangle/tetrahedron, *J. Numer. Math.* 30 (2022), no. 3, 163–172.
- [44] X. Ye and S. Zhang, Order two superconvergence of the CDG method for the Stokes equations on triangle/tetrahedron, *Journal of Applied Analysis and Computation*, 12 (2022), no. 6, 2578–2592.
- [45] X. Ye and S. Zhang, Order two superconvergence of the CDG finite elements on triangular and tetrahedral meshes, *CSIAM Trans. Appl. Math.* 4 (2023), no. 2, 256–274.
- [46] X. Ye and S. Zhang, Four-order superconvergent weak Galerkin methods for the biharmonic equation on triangular meshes, *Communications on Applied Mathematics and Computation*, Doi:10.1007/s42967-022-00201-5, 2023.
- [47] X. Ye and S. Zhang, Four-order superconvergent CDG finite elements for the biharmonic equation on triangular meshes, *J. Comput. Appl. Math.*, 2023, doi: 10.1016/j.cam.2023.115516.
- [48] S. Zhang, An optimal order multigrid method for biharmonic, C^1 finite-element equations, *Numer. Math.* 56 (1989), 613–624.
- [49] S. Zhang, A new family of stable mixed finite elements for the 3D Stokes equations. *Math. Comp.* 74 (2005), no. 250, 543–554.

SCHOOL OF MATHEMATICAL SCIENCE, TONGJI UNIVERSITY, SHANGHAI, 200092, CHINA

INSTITUTE OF COMPUTATIONAL MATHEMATICS, AMSS, CHINESE ACADEMY OF SCIENCES, BEIJING, 100190, CHINA

Email address: `xxj@lsec.cc.ac.cn`

DEPARTMENT OF MATHEMATICAL SCIENCES, UNIVERSITY OF DELAWARE, NEWARK, DE 19716, USA.

Email address: `szhang@udel.edu`